Journal of Energy Chemistry 30 (2019) 84–89

Contents lists available at ScienceDirect

Journal of Energy Chemistry

journal homepage: www.elsevier.com/locate/jechem

http://www.journals.elsevier.com/journal-of-energy-chemistry/

# Naphthalene-modulated microporous carbon layers of $LiFePO_4$ improve the high-rate electrochemical performance

Taotao Huo[a], Ning Nie[a], Yuanyuan Liu[a,c], Jinli Zhang[a,b], Feng Yu[b,*], Wei Li[a,*]

[a] School of Chemical Engineering & Technology, Tianjin University, Tianjin 300350, China
[b] School of Chemical Engineering, Shihezi University, Shihezi 832003, Xinjiang, China
[c] College of Chemistry and Chemical Engineering, Yantai University, Yantai 264005, Shandong, China

ARTICLE INFO

*Article history:*
Received 2 January 2018
Revised 24 March 2018
Accepted 1 April 2018
Available online 5 April 2018

*Keywords:*
Lithium iron phosphate
Carbon coating
Micropore fine-modulation
$Li^+$ diffusion rate
Li-ion batteries

ABSTRACT

Carbon layers with microporous structures fine-modulated by naphthalene (NAP) were prepared to coat on $LiFePO_4$, aiming to enhance the $Li^+$ diffusion coefficient for Li-ion batteries. Characterized by BET, XRD, TEM, EIS, etc., it is indicated that in the presence of NAP, the carbon-coated $LiFePO_4$/C-NAP composites have the enlarged micropore size of 1.66 nm and the enhanced $Li^+$ diffusion coefficient of $2.83 \times 10^{-12}$ $cm^2$ $s^{-1}$, which is about five times higher than that of $LiFePO_4$/C prepared in the absence of NAP. At a high rate of 20 C, the discharge capacity of the $LiFePO_4$/C-NAP is up to 120.1 mA h $g^{-1}$ and maintains a good retention rate of 93.2% after 400 cycles. It is suggested that the NAP-modulated carbon coating is a promising route to accelerate the Li-ion diffusion rate and enhance the electrochemical performance for lithium ion batteries.



## 1. Introduction

The applications of lithium ion batteries have been recently expanding to many fields involving mobile phones, laptops, personal digital assistants, electro mobile and emergency battery box [1–3]. Lithium iron phosphate ($LiFePO_4$, LFP), as one of the most promising cathode materials for lithium ion batteries, has the advantages of high discharging capacity (170 mA h $g^{-1}$), moderate voltage plateau (3.45 V vs. $Li^+$/Li) and environmental friendliness [4,5]. However, LFP has the drawbacks of small electronic conductivity and low Li ion diffusion rate, which retards its large-scale utilizations [6–8]. A number of methods have been reported to improve the electrochemical performance of $LiFePO_4$, involving surface coatings with conductive materials [9–12], modulating the particle size and shape [13–15], adding alien ion dopants [16–18], adjusting unhindered ion-moving channel [19,20].

Among these modification methods, carbon coating has been considered as an effective way to enhance the overall conductivity of LFP. Many efforts have been made to prepare electrode materials with uniform and thin carbon coatings [21], focusing on the graphitization degree of coatings and the carbon contents [12,22]. However, it was reported that the excessive carbon content could result in the lower $Li^+$ diffusion rate and consequently poorer electrochemical performance of LFP/C [23,24]. For example, Lu et al. prepared LFP/C with the carbon content of 8 wt% and high degree graphitization ratio ($I_D/I_G$) of 0.928, which had a capacity of 138 mA h $g^{-1}$ at 0.2 C, with the overall conductivity increased from $10^{-8}$ to $10^{-4}$ S $cm^{-1}$ [25]. While Pratheeksha et al. synthesized LFP/C with a low carbon content (3 wt%) and a graphitization degree of ($I_D/I_G = 0.769$) by dehydration polymerization process, which exhibited a good performance of 167 mA h $g^{-1}$ at 0.1 C [12]. On the other hand, the surface carbon layers incorporated with heteroatoms including P, N and B elements have been reported to augment the electrochemical performance of LFP/C [9,26–28], $SnO_2$, etc. [29,30]. Taking into account the diffusion channel for Li-ions with the radius about 0.68 Å [31], it is intriguing to study whether or not the size of the micropores in carbon coatings on LFP could affect the Li-ion diffusion rate, and consequently influence the electrochemical performance of LFP/C.

Naphthalene is a bicyclic aromatic hydrocarbon with a low sublimation temperature and has been used as a popular foaming agent to generate porous materials [32,33]. For instance, Li et al. utilized naphthalene particles to construct a high-porosity (>50%) ceramic body using the mixture of hydroxyapatite and polymethylmethacrylate, aiming at mimicking the natural structure of bone [34]. Su et al. synthesized the graphitic carbon nanodisks using naphthalene to generate porous structures [35]. In this article, we adopted naphthalene to modulate the size distribution of micropore networks in carbon coatings around LFP, as displayed in Scheme 1, and studied the effect of the narrow size of micropores in carbon coatings on the Li-ion diffusion rate. Characterized by

* Corresponding authors.
*E-mail addresses:* yufeng05@mail.ipc.ac.cn (F. Yu), liwei@tju.edu.cn (W. Li).

https://doi.org/10.1016/j.jechem.2018.04.002

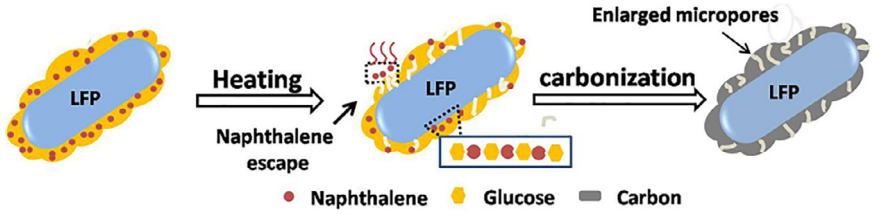


**Scheme 1.** Modulating the size of micropores in carbon coatings of $LiFePO_4$/C via naphthalene.

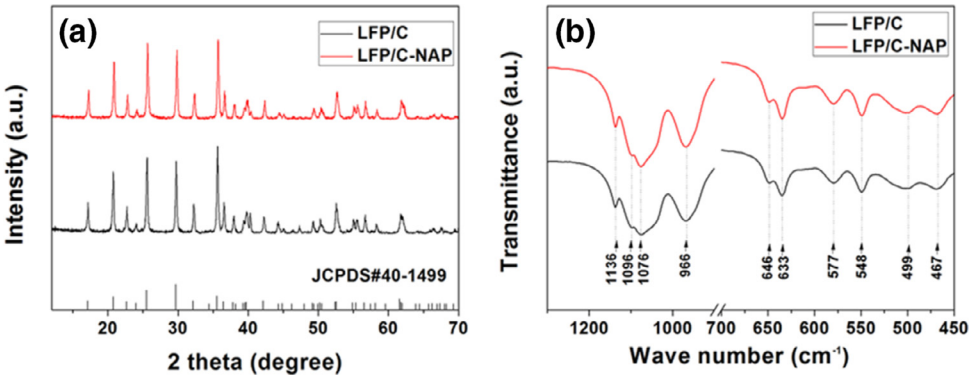


**Fig. 1.** (a) XRD patterns and (b) FT-IR spectra of LFP/C and LFP/C-NAP.

BET, XRD, TEM, EIS, etc., it is illustrated that naphthalene can effectively fine-tune the size of micropores in carbon coatings; in particular, the slightly enlarged micropores in the coating layers results in significant improvement of the electrochemical performance of LFP/C at high rates.

## 2. Experimental

### 2.1. Synthesis of the materials

Lithium iron phosphate was prepared through a one-step solvothermal method using polyethylene glycol 400 (PEG400) according to the following steps: 1.0 mol $L^{-1}$ LiOH aqueous solution was slowly dropped into the mixture solution of $H_3PO_4$ and PEG400 under nitrogen atmosphere with the vigorous stirring rate of $1.3 \times 10^4$ rpm [36]. After 30 min, a 0.5 mol $L^{-1}$ $FeSO_4$ aqueous solution was added into the above mixture with the molar ratio of Li:Fe:P = 3:1:1 to generate the white suspension solution. The whole procedure was operated under a high pure nitrogen atmosphere. The obtained suspension solution was put in an autoclave and heated to 180 °C with a rising rate of 3 °C $min^{-1}$. After 9 h the prepared mixture was cooled down to the room temperature, followed by filtration and desiccation at 120 °C for 12 h to obtain the particles of $LiFePO_4$.

$LiFePO_4$ was coated with carbon layers using glucose as the carbon source and naphthalene as the pore-forming agent. Without the additive of naphthalene, 2 g $LiFePO_4$ particles were mixed with 0.34 g glucose and 2 mL ethanol, followed by ball-milling at 500 rpm for 2 h and then dried at 40 °C for 10 h. The mixture was calcined at 600 °C for 5 h with a heating rate of 5 °C $min^{-1}$ under nitrogen atmosphere to obtain the carbon-coated $LiFePO_4$, denoted as LFP/C.

To modulate the pore size in carbon coating layers, certain amount of naphthalene (NAP) (with the ratio NAP/LFP of 10 wt%) was added into the ball-milling mixture, following the same procedure as that of LFP/C. The final obtained sample was named as LFP/C-NAP.

### 2.2. Materials characterization

The obtained materials were characterized by X-ray powder diffraction (XRD, Rigaku D/max 2500 V/PC) through Cu-$K\alpha$ radiation source in the angle range of 15°–75°. The FTIR spectra of the samples were recorded on a Nicolet iZ10 spectrometer (Thermo scientific) from 4000 to 400 $cm^{-1}$ at room temperature. Raman spectra were carried out on Renishaw via reflex Raman spectrometer with a laser of 532.4 nm. Scanning electron microscopy (SEM) images were observed by a Hitachi S4800 microscope (INSA, Lyon). HR-TEM images were performed under a JEM-100CX-IIinstrument running at 100 kV. Thermogravimetric (TG) analysis was performed in air atmosphere on a Netzsch-STA 449C, operating from 20 to 700 °C at a heating rate of 10 °C $min^{-1}$. Textural properties including the pore volume and pore size were measured using $N_2$ adsorption–desorption isotherms through Quantachrome autosorb $iQ_2$ automated gas sorption analyzer.

### 2.3. Electrochemical measurements

Electrochemical tests were employed using CR2032 coin cells at room temperature with the metallic lithium as the anode. The mixture of the cathode material was prepared in N-methylpyrrolidinone solution by sufficiently mixing LFP/C or LFP/C-NAP, polyvinylidene fluoride and the acetylene black with the mass ratio of 8:1:1. After stirring for 10 h, the slurry was coated on the aluminum foils and then transferred into the vacuum oven dried at 120 °C for 12 h. All electrodes were cut into disks with a diameter of 1.3 cm. The average mass loading of active material was about 2.13 mg $cm^{-2}$. The electrolyte was the mixture of ethylene carbonate (EC) – dimethyl carbonate (DMC) (with the volume ratio of 1:1) and 1.0 mol $L^{-1}$ $LiPF_6$ solution. The coin-cell was assembled in the argon filled glove box with the water and oxygen content less than 0.1 ppm and the Celgard 2400 as the separator. The charging–discharging performance was measured on the LAND-CT2011A battery testing system (Wuhan, China) in an electrochemical window of 2.0–4.2 V. The (EIS) was characterized through CHI660E (CH Instruments, China), adjusting amplitude signal at 5 mV and frequency range of 0.1 Hz–100 kHz.

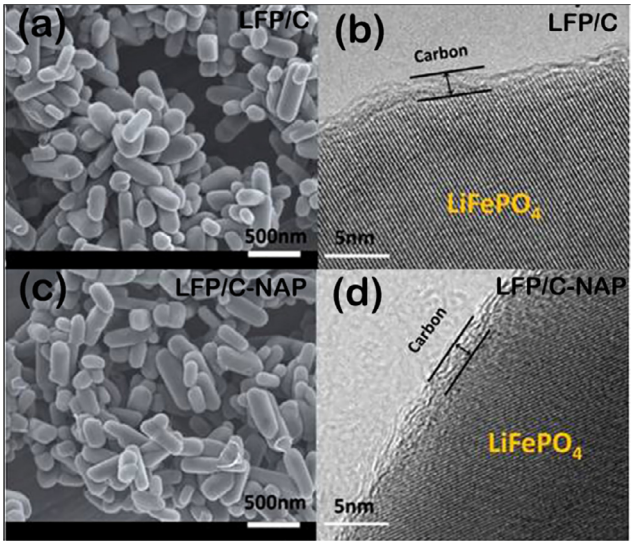


**Fig. 2.** SEM and HR-TEM images of LFP/C (a, b), and LFP/C-NAP (c, d).

## 3. Results and discussion

Fig. 1(a) shows XRD patterns of LFP/C and LFP/C-NAP samples. Both of them show strong and narrow diffraction peaks attributed to the olivine-type $LiFePO_4$ phase with a space group of Pnma (JCPDS card NO.40-1499), reflecting high phase purity of crystalline $LiFePO_4$ for both LFP/C and LFP/C-NAP. Moreover, FTIR spectra also indicate the similar structure of LFP/C and LFP/C-NAP. As shown in Fig. 1(b), the peaks at 1136, 1096, 1075, and 966 $cm^{-1}$ correspond to the stretching vibrations of the $PO_4^{3-}$ units in LFP [37]. The peaks at 499 and 467 $cm^{-1}$ are due to the translational vibrations of lithium ions adjacent to the oxygen atoms in the olivine $LiFePO_4$ structure [38]. Thus, the additive of NAP shows no effect on the crystallinity of $LiFePO_4$.

SEM and HR-TEM images were carried out to compare the morphology of LFP/C-NAP and LFP/C. As shown in Fig. 2, SEM images indicate nanoparticles with similar rod-like shape and the length × width about 300–500 nm × 100 nm in the presence and the absence of naphthalene. HR-TEM images illustrate that the carbon coating on these samples has the thickness about 2 nm, and the interplanar spacing areas of the bulk material can be clearly observed.

According to the TG analysis in Fig. S1, the carbon content is calculated as 6.67% for the sample LFP/C, and 6.66% for LFP/C-NAP, indicating that the NAP additive has little effect on the amount of carbon coatings. On the other hand, Raman spectra of these samples show two distinct peaks at 1325 and 1595 $cm^{-1}$ attributed to the D-band (Disordered band) and the G-band (Graphitized band), respectively (Fig. 3). The D band is characteristic of the disordered structure ascribed to the breathing vibration at the boundary of grapheme sheet, whereas the G band is corresponding to bond stretching of the graphitized carbon atoms. The intensity ratio of the D band to G band ($I_D/I_G$) has been widely applied to evaluate the graphitization degree of the carbon materials [39,40]. As listed in Fig. 3, the $I_D/I_G$ ratios equal 0.83–0.82 for these samples, suggesting that LFP/C-NAP and LFP/C have similar graphitization degree of carbon coatings.

Fig. 4 shows the nitrogen adsorption/desorption isotherms for both samples, corresponding to type-IV isotherms of the IUPAC classification. In particular the pore size distribution of LFP/C-NAP is wider obviously than that of LFP/C, as displayed by the inset of Fig. 4. The pore size distribution in the thin carbon coating layers was analyzed using Dubinin–Astakhov (D–A) equation

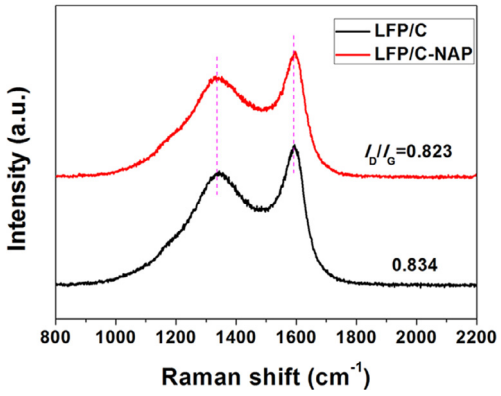


**Fig. 3.** Raman spectra for LFP/C and LFP/C-NAP.

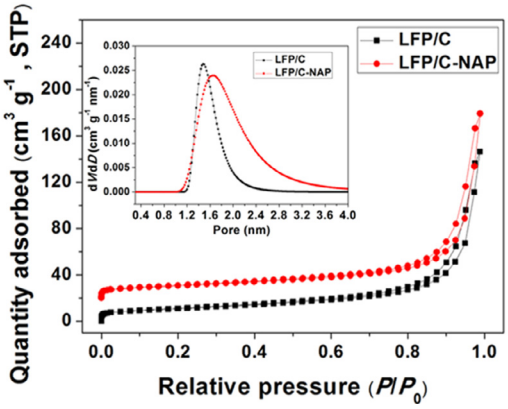


**Fig. 4.** Nitrogen adsorption/desorption isotherms and pore size distributions for the samples.

**Table 1.** Specific surface structure determined by Dubinin–Astakhov equation.

| Sample | Micropore surface area ($m^2\ g^{-1}$) | Micropore volume ($cm^3\ g^{-1}$) | Modal pore size (nm) |
|---|---|---|---|
| LFP/C | 52 | 0.012 | 1.48 |
| LFP/C-NAP | 45 | 0.024 | 1.66 |

[41–43]. As listed in Table 1, LFP/C shows the micropore volume of 0.012 $cm^3\ g^{-1}$ and the modal pore size of 1.48 nm, while LFP/C-NAP has high micropore volume of 0.024 $cm^3\ g^{-1}$ (twice as that of LFP/C) and the enlarged modal pore size of 1.66 nm (12% higher than that of LFP/C).

The electrochemical performances of LFP/C and LFP/C-NAP were tested and shown in Fig. 5. At the rate of 0.1 C, two samples display stable charging–discharging voltage platform at 3.45 V (vs. $Li^+/Li$), which is attributed to the phase redox reaction of $LiFePO_4$ and $FePO_4$ (Fig. 5(a) and (b)). The initial discharge capacity of the sample LFP/C and LFP/C-NAP is 145.9 and 161.1 mA h $g^{-1}$ respectively, and the corresponding coulombic efficiency is 84.7% and 93.6%. Under higher current rates of 1–20 C, LFP/C-NAP shows superior electrochemical property comparing with LFP/C. LFP/C-NAP has the discharge capacity of 142.2 mA h $g^{-1}$ at 1 C, and 120.1 mA h $g^{-1}$ at 20 C, much higher than LFP/C (127.5 mA h $g^{-1}$ at 1 C and 102.9 mA h $g^{-1}$ at 20 C) (Fig. 5(c)). The rate capacity retention of LFP/C-NAP and LFP/C is respectively 88.3% and 87.4% at 1 C, decreasing to 74.5% and 70.5% at 20 C (Fig. 5(d)). As a control, the performance of LFP without carbon coating was measured, as shown in Fig. S2, the initial discharge capacity of uncoated LFP is respectively 90.0, 51.3, and 20.8 mA h $g^{-1}$ at the rate of 0.1, 1 and 20 C, far inferior to LFP/C and LFP/C-NAP. Therefore, the superior electrochemical performance of LFP/C-NAP is greatly asso-

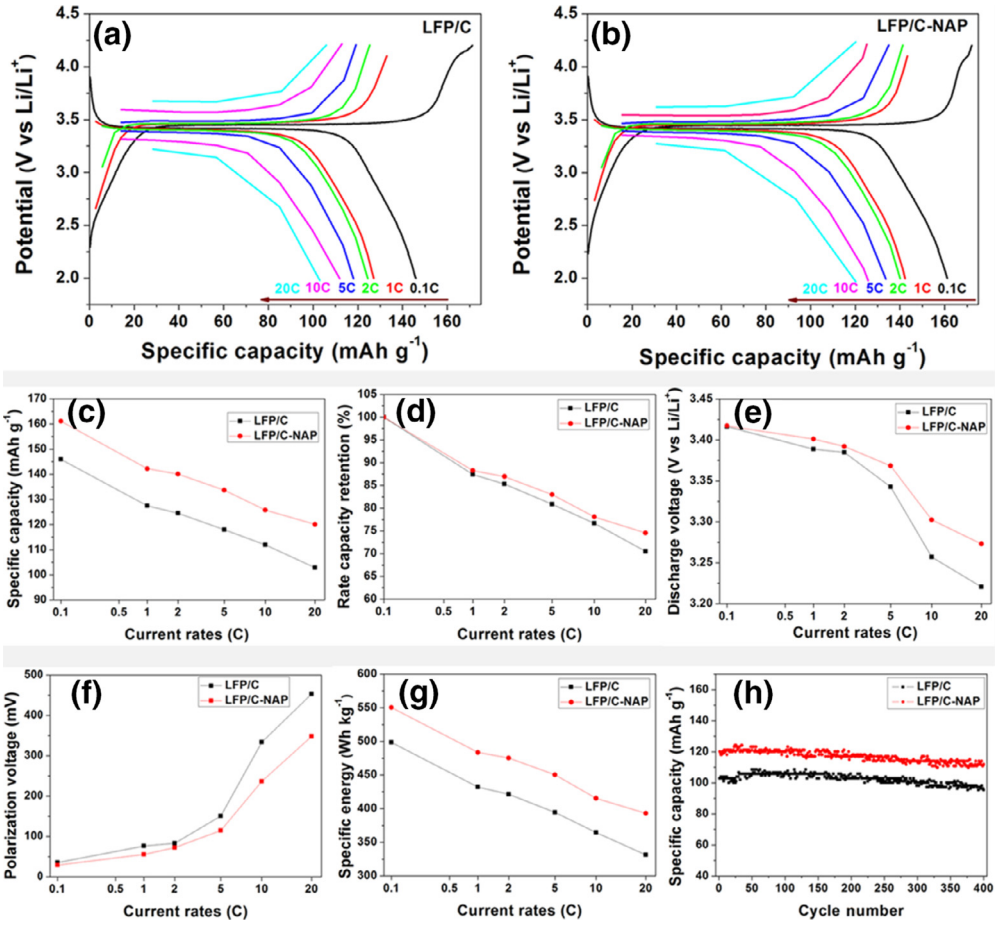


**Fig. 5.** The electrochemical performance for samples LFP/C and LFP/C-NAP: (a, b) The charge–discharge profiles, (c) the capacity at various *C* rates, (d) retention of discharge specific capacity, (e) polarization voltage obtained from the phase transition peaks of differential capacity (d*Q*/d*V*) as a function of potential (*V*) for two samples at various *C* rates, (f) discharge voltage, (g) specific energy, (h) the cycle performance at 20 C.

ciated with the carbon coating layers as well as the size of the micropores in the coating layers.

In order to investigate the polarization voltage gap during charging–discharging process, d*Q*/d*V* (*Q* and *V* are the capacity and the voltage of the cells), calculated from the data in charge-discharge curves, were employed at different rates to get the gap of polarization voltage. As displayed in Fig. 5(e), the polarization voltage gap of LFP/C is larger than that of LFP/C-NAP, increasing with the current rates. Noteworthy, larger polarization can cause lower discharge voltage, and then lead to smaller specific energy [44]. The specific energy is respectively 498.4 and 550.5 W h $kg^{-1}$ for LFP/C and LFP/C-NAP at 0.1 C, corresponding to the discharge voltage of 3.411 and 3.418 V, respectively. At 0.1 C the specific energy of LFP/C-NAP reaches 95.2% of the theoretical specific energy (578 W h $kg^{-1}$), much higher than that of LFP/C (86.2%), whereas at 20 C the specific energies of LFP/C-NAP and LFP/C decrease to 68.0% and 57.2%, respectively. Fig. 5(h) displays the cycling performance of two samples at 20 C. After 400 charging–discharging cycles the discharging capacity is respectively 95.4 and 111.9 mA h $g^{-1}$ for LFP/C and LFP/C-NAP, with the capacity retention of 92.7% and 93.2% compared with the correspondingly initial capacity. It is confirmed that the enlarged micropores in carbon coating layers of LFP/C-NAP are beneficial to improve the specific capacity but also the cycling performance of LFP, in particular at high rates.

Cyclic voltammetry (CV) at various scan rates (0.1–3.5 mV $s^{-1}$) was tested to study the kinetic behavior of LFP/C and LFP/C-NAP. As shown in Fig. 6(a) and (b), all the curves have one pair of redox peaks corresponding to $Fe^{2+}/Fe^{3+}$ couples around 3.4 V vs. $Li^+/Li$, reflecting the fact of high phase purity for samples. With the increase of the scan rate, the positive peak and the negative peak shift in opposite direction for both LFP/C and LFP/C-NAP, illustrating that the polarization increases with the charge-discharge rate. Fig. 6(c) shows CV profiles for LFP/C and LFP/C-NAP at 0.1 mV $s^{-1}$, indicating that the oxidation and reduction peaks are located at 3.475/3.390 V for LFP/C-NAP while at 3.484/3.385 V for LFP/C. It is suggested that LFP/C-NAP exhibits a better reversibility of the electrode reaction.

Fig. 6(d) shows the peak current during anodic ($I_p$) in direct proportion the square root of voltage scan rate ($v^{1/2}$) and the slope of LFP/C-NAP (0.1734) is larger than that of LFP/C (0.1278). Therefore, the Li-ion diffusion coefficient *D* for samples can be calculated by the Randles Sevcik equation [31,45]:

$$I_P = 2.69 \times 10^5 n^{3/2} A D^{1/2} C \upsilon^{1/2}$$

where $I_p$ is the peak current (A), *n* is the charge transfer number in the electrode reaction, *A* is the area of electrode (1.32 $cm^2$), *C* is the $Li^+$ concentration (mol $cm^{-3}$), *D* is the Li-ion diffusion coefficient ($cm^2$ $s^{-1}$), and $\upsilon$ is the scan rate (V $s^{-1}$). According to the slopes of fitted results, the Li-ion diffusion coefficient *D* for LFP/C and LFP/C-NAP is respectively $2.53 \times 10^{-10}$ $cm^2$ $s^{-1}$ and $4.59 \times 10^{-10}$ $cm^2$ $s^{-1}$, with the corresponding *R*-square of 99.1% and 99.0%, suggesting that the structure of LFP/C-NAP is beneficial to the fast diffusion of lithium ions.

The electrochemical impedance spectroscopy (EIS) of the materials is also carried out to further investigate $Li^+$ transport kinetics and internal resistance. Moreover, the EIS can offer a more

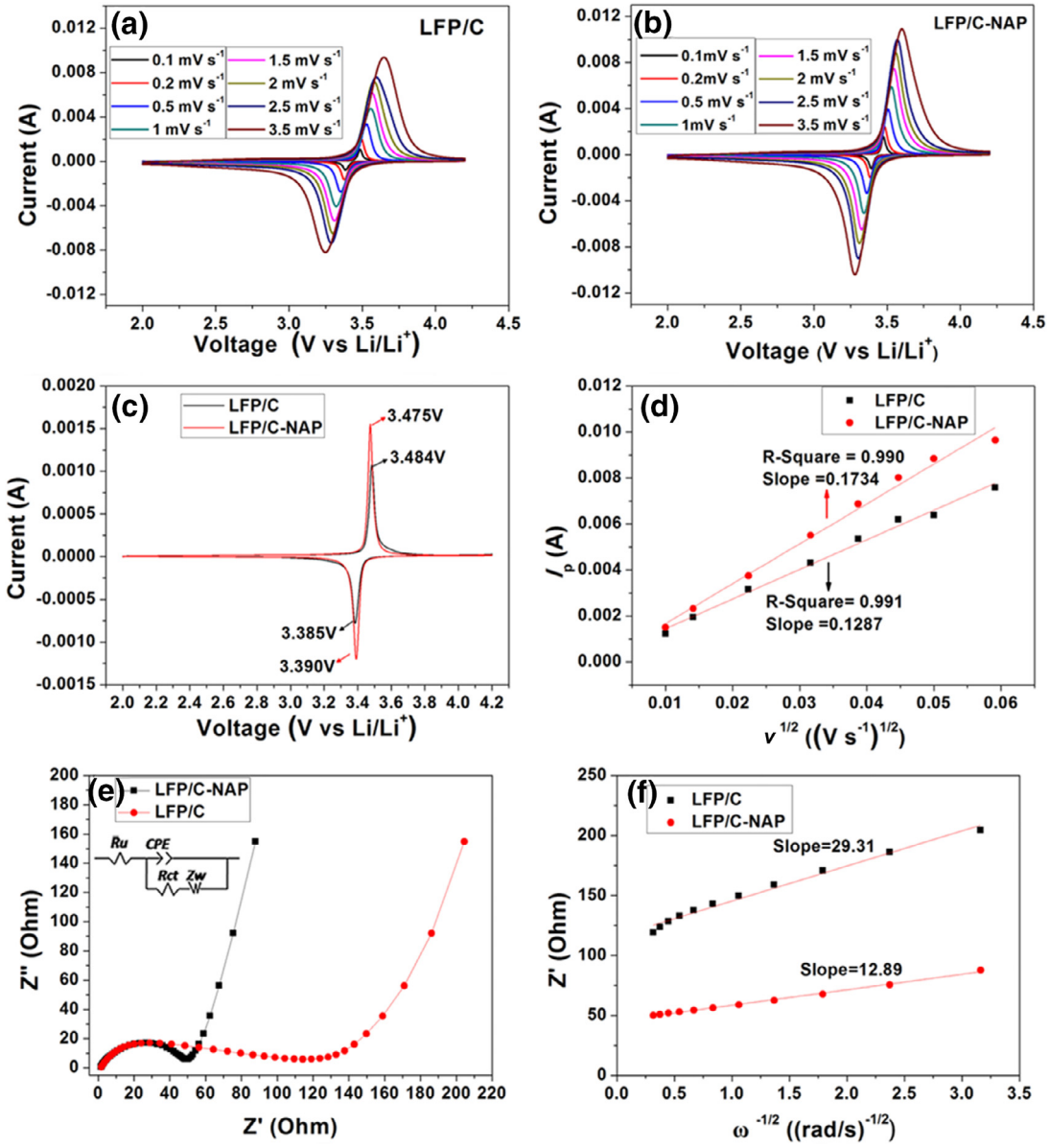


**Fig. 6.** (a, b) Cyclic voltammograms for LFP/C and LFP/C-NAP at different scan rates, (c) cyclic voltammograms for LFP/C and LFP/C-NAP at scan rate of 0.1 mV $s^{-1}$, (d) the relationship between $I_p$ and square root of potential scan rate, (e) the equivalent circuit and EIS of LFP/C and LFP/C-NAP, (f) the relationship between $Z'$ and reciprocal square root of frequency ($\omega^{-1/2}$).

accurate determination of the diffusion coefficient, since the interfacial and diffusion processes are usually separated on the frequency scale. The equivalent circuit diagram simulated through the Zview software is displayed in Fig. 6(e), where Ru refers to the uncompensated resistances including the particle-particle contact resistance, the electrolyte resistance, and the resistance between the electrode and the current collector. $R_{ct}$ represents the charge transfer resistance concerning the electrochemical reaction at the electrode-electrolyte interface and particle-particle contact [46,47]. CPE stands for the scatter effect of the constant phase element. As shown in Fig. 6(e), the semicircle in high-frequent district is attributed to the charge-transfer process during the electrode reaction, while the oblique line in the low-frequent region refers to the moving of the $Li^+$ between the electrode (Warburg diffusion Zw). It is clear that the semicircle of the LFP/C-NAP is smaller than that of LFP/C material, and the values of $R_{ct}$ are respectively 123 Ω and 49 Ω for samples LFP/C and LFP/C-NAP. Therefore, the carbon coating with enlarged micropores around LFP can decrease the charge transfer resistance and improve the dynamic restriction. Meanwhile, the lithium ion diffusion coefficients ($D_{Li^+}$) are calculated by the following equation:

$$D = \frac{R^2T^2}{2A^2n^2F^4C^2\sigma^2}$$

where $R$ is the constant of gas (8.315 J $mol^{-1}$ $K^{-1}$), $T$ represents the room temperature (298.15 K), $n$ is the number of charge (discharge) per molecular reaction, $F$ is the Faraday constant, $C$ is the $Li^+$ concentration, and $\sigma$ is the Warburg factor correlate with $Z'$:

$$Z' = R_D + R_L + \sigma\omega^{-1/2}$$

Fig. 6(f) shows the line concerning $Z'$ and $\omega^{(-1/2)}$ in low-frequency district. By calculation, the lithium ion diffusion coefficient of LFP/C and LFP/C-NAP is respectively $5.46 \times 10^{-13}$ and $2.83 \times 10^{-12}$ $cm^2$ $s^{-1}$, further confirming the fast lithium ion migration in LFP/C-NAP. Compared with the reports in existing literature, such as $1.43 \times 10^{-13}$ $cm^2$ $s^{-1}$ for LFP/C-H1.3 [36],

$12.6 \times 10^{-14}$ cm$^2$ s$^{-1}$ for $LiFe_{0.98}PO_4$/C [48], $6.29 \times 10^{-14}$ cm$^2$ s$^{-1}$ for $LiFe_{0.97}Mn_{0.03}PO_4$/C [18], NAP fine-modulated micropores in carbon layer can drastically improve Li-ion transfer efficiency. The above-mentioned results confirm that the sample with enlarged micropore carbon coating can establish more unrestricted pathways for $Li^+$ passing through during charging–discharging, which exhibits more excellent electrochemical performance.

## 4. Conclusions

A naphthalene(NAP)-promoted procedure has been developed to fine-modulate the microporous structure of carbon coatings on $LiFePO_4$. It is indicated that the carbon coatings around LFP/C-NAP have the micropores with the modal size enlarged by 12% and high micropore volume twice as that of the LFP/C. For the LFP/C-NAP the $Li^+$ diffusion rate is as high as $2.83 \times 10^{-12}$ cm$^2$ s$^{-1}$, greatly larger than that of LFP/C ($5.46 \times 10^{-13}$ cm$^2$ s$^{-1}$). At a high rate of 20 C, the LFP/C-NAP can maintain the discharge capacity of 120.1 mA h g$^{-1}$ with a good retention rate of 93.2% after 400 cycles. The results suggested that the fine-modulation of microporous structure of carbon coatings on LFP is an effective route to accelerate the Li-ion diffusion coefficient in $LiFePO_4$/C, and then enhance the electrochemical performance for lithium-ion batteries.

## Acknowledgments

This work was financially supported by the National Natural Science Foundation of China (Nos. 21476158, 21621004), and Program for Changjiang Scholars and Innovative Research Team in University (No. IRT_15R46).

## Supplementary materials

Supplementary material associated with this article can be found, in the online version, at doi:10.1016/j.jechem.2018.04.002.

## References

[1] D. Deng, Energy Sci. Eng. 3 (2015) 385–418.
[2] L. Lu, X. Han, J. Li, J. Hua, M. Ouyang, J. Power Sources 226 (2013) 272–288.
[3] K. Zhang, Z. Hu, J. Chen, J. Energy Chem. 22 (2013) 214–225.
[4] X.Q. Ou, H.C. Gu, Y.C. Wu, J.W. Lu, Y.J. Zheng, Electrochim. Acta 96 (2013) 230–236.
[5] X. Lei, H. Zhang, Y. Chen, W. Wang, Y. Ye, C. Zheng, P. Deng, Z. Shi, J. Alloys Compd. 626 (2015) 280–286.
[6] A.S. Andersson, J.O. Thomas, B. Kalska, L. Haggstrom, Electrochem. Solid State Lett. 3 (2000) 66–68.
[7] C. Delacourt, L. Laffont, R. Bouchet, C. Wurm, J.B. Leriche, M. Morcrette, J.M. Tarascon, C. Masquelier, J. Electrochem. Soc. 152 (2005) A913–A921.
[8] A. Banday, S. Murugavel, J. Appl. Phys. 121 (2017) 045111.
[9] J.L. Zhang, N. Nie, Y.Y. Liu, J. Wang, F. Yu, J.J. Gu, W. Li, ACS Appl. Mater. Interfaces 7 (2015) 20134–20143.
[10] J.L. Zhang, J. Wang, Y.Y. Liu, N. Nie, J.J. Gu, F. Yu, W. Li, J. Mater. Chem. A 3 (2015) 2043–2049.
[11] P. Wang, G. Zhang, Z. Li, W. Sheng, Y. Zhang, J. Gu, X. Zheng, F. Cao, ACS Appl. Mater. Interfaces 8 (2016) 26908–26915.
[12] P.M. Pratheeksha, E.H. Mohan, B.V. Sarada, M. Ramakrishna, K. Hembram, P.V. Srinivas, P.J. Daniel, T.N. Rao, S. Anandan, Phys. Chem. Chem. Phys. 19 (2016) 175–188.
[13] Y.Y. Liu, J.J. Gu, J.L. Zhang, F. Yu, J. Wang, N. Nie, W. Li, RSC Adv. 5 (2015) 9745–9751.
[14] H.L. Zou, G.H. Zhang, P.K. Shen, Mater. Res. Bull. 45 (2010) 149–152.
[15] Y. Gao, K. Chen, H. Chen, X. Hu, Z. Deng, Z. Wei, J. Energy Chem. 26 (2017) 564–568.
[16] L.J. Pang, M.S. Zhao, X. Zhao, Y.J. Chai, J. Power Sources 201 (2012) 253–258.
[17] F. Lu, Y.C. Zhou, J. Liu, Y. Pan, Electrochim. Acta 56 (2011) 8833–8838.
[18] C. Li, G. Li, X. Guan, J. Energy Chem. 26 (2017) 1–7.
[19] K.-Y. Park, I. Park, H. Kim, G. Yoon, H. Gwon, Y. Cho, Y.S. Yun, J.-J. Kim, S. Lee, D. Ahn, Y. Kim, H. Kim, I. Hwang, W.-S. Yoon, K. Kang, Energy Environ. Sci. 9 (2016) 2902–2915.
[20] G. Hu, P. Chen, Z. Liu, Y. Cao, Z. Zhang, Z. Peng, D. Ke, J. Alloys Compd. 696 (2017) 177–184.
[21] L. Zhang, G. Zhang, H.B. Wu, L. Yu, X.W. Lou, Adv. Mater. 25 (2013) 2589–2593.
[22] J. Song, B. Sun, H. Liu, Z. Ma, Z. Chen, G. Shao, G. Wang, ACS Appl. Mater. Interfaces 8 (2016) 15225–15231.
[23] Y. Wang, B. Zhu, Y. Wang, F. Wang, Ceram. Int. 42 (2016) 10297–10303.
[24] W. Li, J. Hwang, W. Chang, H. Setiadi, K.Y. Chung, J. Kim, J. Supercrit. Fluids 116 (2016) 164–171.
[25] C.-Z. Lu, G.T.-K. Fey, H.-M. Kao, J. Power Sources 189 (2009) 155–162.
[26] C. Wang, Z.Y. Guo, W. Shen, Q.J. Xu, H.M. Liu, Y.G. Wang, Adv. Funct. Mater. 24 (2014) 5511–5521.
[27] E. Avci, M. Mazman, D. Uzun, E. Bicer, T. Sener, J. Power Sources 240 (2013) 328–337.
[28] J. Yang, J. Wang, X. Li, D. Wang, J. Liu, G. Liang, M. Gauthier, Y. Li, D. Geng, R. Li, X. Sun, J. Mater. Chem. 22 (2012) 7537.
[29] X.Y. Zhou, L. Yu, X.W Lou, Adv. Energy Mater. 6 (2016) 1600451.
[30] E.-J. Oh, R. Hempelmann, V. Nica, I. Radev, H. Natter, J. Power Sources 341 (2017) 240–249.
[31] J. Tu, K. Wu, H. Tang, H. Zhou, S. Jiao, J. Mater. Chem. A 5 (2017) 17021–17028.
[32] S.R. Dash, R. Sarkar, S. Bhattacharyya, Ceram. Int. 41 (2015) 3775–3790.
[33] S. Vijayan, R. Narasimman, K. Prabhakaran, Ceram. Int. 41 (2015) 1487–1494.
[34] S.H. Li, J.R. Wijn, P. Layrolle, K. Groot, J. Am. Ceram. Soc. 86 (2002) 65–72.
[35] P. Su, L. Jiang, J. Zhao, J. Yan, C. Li, Q. Yang, Chem. Commun. 48 (2012) 8769–8771.
[36] Y.Y. Liu, J.J. Gu, J.L. Zhang, J. Wang, N. Nie, Y. Fu, W. Li, F. Yu, Electrochimica. Acta 173 (2015) 448–457.
[37] A. Ait Salah, P. Jozwiak, K. Zaghib, J. Garbarczyk, F. Gendron, A. Mauger, C.M. Julien, Spectrochim. Acta. A: Mol. Biomol. Spectrosc. 65 (2006) 1007–1013.
[38] C.M. Burba, R. Frech, J Electrochem. Soc. 151 (2004) A1032.
[39] Y.L. Liu, C.X. Pan, J.B. Wang, J. Mater. Sci. 39 (2004) 1091–1094.
[40] W. Li, H. Zhang, C. Wang, Y. Zhang, L. Xu, K. Zhu, S. Xie, Appl. Phys. Lett. 70 (1997) 2684–2686.
[41] S. Furmaniak, A.P. Terzyk, P.A. Gauden, P.J.F. Harris, P. Kowalczyk, J. Phys.: Condens. Mater. 22 (2010) 1–10.
[42] R.K. Vyas, Shashi, S. Kumar, Indian J. Chem. Technol. 11 (2004) 704–709.
[43] A.P. Terzyk, P.A. Gauden, P. Kowalczyk, Carbon 40 (2002) 2879–2886.
[44] F. Yu, S.H. Lim, Y. Zhen, Y. An, J. Lin, J. Power Sources 271 (2014) 223–230.
[45] J. He, H. Zhong, J. Wang, L. Zhang, J Alloys Compd. 714 (2017) 409–418.
[46] L. He, W. Zha, D. Chen, J. Alloys Compd. 727 (2017) 948–955.
[47] G. Wu, R. Ran, B. Zhao, Y. Sha, C. Su, Y. Zhou, Z. Shao, J. Energy Chem. 23 (2014) 363–375.
[48] Y. Feng, J. Gu, F. Yu, C. Lin, J. Zhang, N. Nie, W. Li, RSC Adv. 7 (2017) 33544–33551.